A peer-reviewed version of this preprint was published in PeerJ on 28 July 2015.

Silva PJ, Rodrigues V. 2015. Mechanistic pathways of mercury removal from the organomercurial lyase active site. PeerJ 3:e1127 https://doi.org/10.7717/peerj.1127

Mechanistic pathways of mercury removal from the organomercurial lyase active site

Pedro Silva, Viviana Rodrigues

Bacterial populations present in Hg-rich environments have evolved biological mechanisms to detoxify methylmercury and other organometallic mercury compounds. The most common resistance mechanism relies on the H^+-assisted cleavage of the Hg-C bond of methylmercury by the organomercurial lyase MerB. Although the initial reaction steps which lead to the loss of methane from methylmercury have already been studied experimentally and computationally, the reaction steps leading to the removal of Hg^{2+} from MerB and regeneration of the active site for a new round of catalysis have not yet been elucidated. In this paper, we describe an MP2/CBS//B3PW91/6-31G(d) study of the final steps of the reaction catalyzed by MerB. While conceptually simple, these reaction steps occur in a complex potential energy surface where several distinct pathways are accessible and may operate concurrently. The only pathway which clearly emerges as forbidden in our analysis is the one arising from the sequential addition of two thiolates to the metal atom, due to the accumulation of negative charges in the active site. Addition of two thiols, in contrast, leads to two feasible mechanistic possibilities. The most straightforward pathway proceeds through proton transfer from the attacking thiol to Cys159 , leading to its removal from the mercury coordination sphere, followed by a slower attack of a second thiol, which removes Cys96. The other pathway involves Asp99 in an accessory role similar to the one observed earlier for the initial stages of the reaction and affords a lower activation enthalpy, around 14 $kcal.mol^{-1}$, determined solely by the cysteine removal step rather than by the thiol ligation step. Addition of one thiolate to the intermediates arising from either thiol attack occurs without a barrier and produces an intermediate bound to one active site cysteine and from which $Hg(SCH_3)_2$ may be removed only after protonation by solvent-provided H_3O^+. Thiolate addition to the active site (prior to any attack by thiols) leads to pathways where the removal of the first cysteine becomes the rate-determining step, irrespective of whether Cys159 or Cys96 leaves first. Comparisons with the recently computed mechanism of the related enzyme MerA further underline the important role of Asp99 in the energetics of the MerB reaction.

Pedro J. Silva and Viviana A. B. Rodrigues

FP-ENAS/Fac. de Ciências da Saúde, Univ. Fernando Pessoa, Rua Carlos da Maia, 296, 4200-150

Porto-Portugal

PeerJ PrePrints | https://dx.doi.org/10.7287/peerj.preprints.909v1 | CC-BY 4.0 Open Access | rec: 19 Mar 2015, publ: 19 Mar 2015

Introduction

Mercury is naturally present in the environment, especially at specific geologically enriched regions along tectonical plate boundaries (Varekamp & Buseck, 1986), where it can be found as the characteristically colored cinnabar ores (HgS). Though quite insoluble in water (≈10 μg/L), the solubilized species (Hg^{2+}) may be readily uptaken by methanogens and sulfate-reducing bacteria, which then methylate it to methylmercury (Barkay, Miller & Summers, 2003; Lin, Yee & Barkay, 2012) through the combined action of the reductive acetyl-CoA pathway (Choi, Chase & Bartha, 1994) and two novel proteins: a methyl-binding corrinoid-containing protein (HgcA) and a corrinoid-reducing protein with unknown physiological function(Parks et al., 2013). The methylmercury thus formed is highly soluble in lipids and therefore tends to accumulate in living tissues and to be concentrated along the food chain. The solution reactivity of mercury towards soft ligands(Riccardi et al., 2013) like the thiols present in cysteine-containing proteins is responsible for the high toxicity of methylmercury(Eto, Marumoto & Takeya, 2010), especially towards lipid-enriched cells (like those of the nervous system) where its solubility is the highest. Bacterial populations present in Hg-rich environments have therefore evolved biological mechanisms to detoxify methylmercury and other organometallic mercury compounds. The most common resistance mechanism relies on proton-assisted cleavage of the Hg-C bond of methylmercury by the organomercurial lyase MerB(Begley, Walts & Walsh, 1986a,b), and sequential transfer of the remaining Hg^{2+} ion to a flavoprotein (MerA) which reduces the cation to its metallic form(Fox & Walsh, 1982; Ledwidge et al., 2005, 2010).

Extensive experimental studies(Begley et al., 1986a,b; Pitts & Summers, 2002)·(Di Lello et al., 2004; Lafrance-Vanasse et al., 2009) have elucidated the structure of MerB and established that this enzyme does not require any cofactors and uses two thiols (like cysteine or glutathione, but not

dithiothreytol(Pitts & Summers, 2002)) as co-reactants for every mercury organic compound cleaved. A pioneering computational study(Parks et al., 2009) has shown that in the active site any one of two conserved Cys residues (Cys 96 and Cys 159) may, upon deprotonation, complex the Hg moiety of the substrate. A proton is then transferred from the other conserved Cys to a conserved acidic residue (Asp 99), which subsequently acts as a proton donor to the leaving alkyl or aryl group. That study did not, however, address the reaction steps leading to the loss of Hg^{2+} from MerB and regeneration of the active site for a new round of catalysis.

Methods

The active site geometry was built from PDB:3F0P, the crystal structure of the mercury-bound form of MerB(Lafrance-Vanasse et al., 2009). The active site included the conserved residues Cys96, Asp 99, Cys 159, the mercury ion and Hg-complexing water molecule. To prevent unrealistic motions of the active site, the Cα and Cβ atoms of every aminoacid were constrained to their crystallographic positions. All calculations were performed at the B3PW91 level of theory(Perdew, 1991; Becke, 1993), which has been commonly used in the study of Hg-containing complexes(Barone et al., 1997; Ni et al., 2006; Parks et al., 2009; Li et al., 2010; Riccardi et al., 2013). Autogenerated delocalized coordinates(Baker, Kessi & Delley, 1996) were used for geometry optimizations, using the SDD effective core-potential and associated basis set(Küchle et al., 1991) for Hg and the 6-31G(d) basis set for all other atoms. More accurate DFT energies of the optimized geometries were calculated with a triple-ζ quality basis set, 6-311+G(d). Zero point (ZPE) and thermal effects (T=298.15 K, P=1 bar) were evaluated using a scaling factor of 0.9804 for the computed frequencies. All computations were performed with the Firefly quantum chemistry package, which is based Environmental contributions to the energies of the stationary points and transition states were computed with the polarizable

conductor model(Tomasi & Persico, 1994; Mennucci & Tomasi, 1997; Cossi et al., 1998), with dielectric constants ranging from 4 (usually chosen for protein-embeded active sites) to 78.36 (mimicking a completely exposed active site). Dispersion and repulsion effects were evaluated as described by Amovilli and Mennucci(Amovilli & Mennucci, 1997). MP2 single-point energies were computed on the optimized geometries using the aug-cc-pVDZ-PP (or aug-ccpVTZ-PP) basis set(Peterson & Puzzarini, 2005) for mercury and cc-pVDZ (or cc-pVTZ basis sets) for all other elements, and extrapolated to the complete basis set limit (CBS-MP2) as described by Truhlar(Truhlar, 1998). Solution MP2 values were obtained by applying the DFT solvation energies to the gas-phase CBS-MP2 energies.

Results

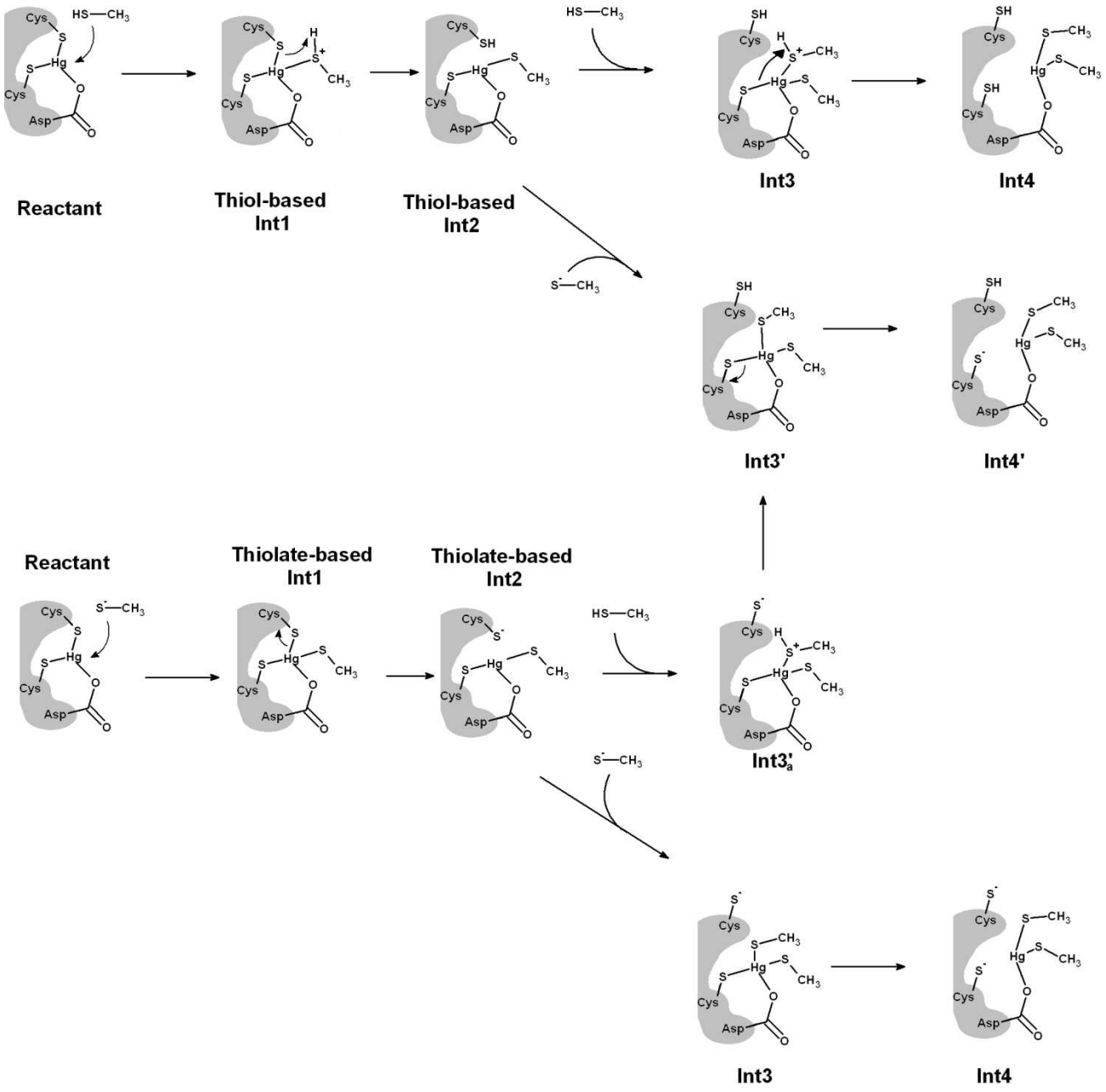

Figure 1: Pathways for Hg removal from MerB, starting from an attacking thiol ("thiol-based" mechanism) or an attacking thiolate ("thiolate-based" mechanism). In both mechanisms, primed-

numbered intermediates arise from the attack of a thiol and a thiolate, whereas intermediates numbered with unprimed numbers arise from the attack of two species with the same protonation state (either two thiols or two thiolates).

A large number of mechanistic pathways for Hg^{2+} removal from the active site of MerB is possible (Fig. 1), depending on the protonation state of each mercury-attacking ligand (thiol vs. thiolate), on whether Cys96 or Cys159 is first ejected from the coordination sphere of the Hg ion, and on whether the protonation state of Asp99 changes throughout the cycle. Our density-functional computations show that extraneous methanethiol is not nucleophilic enough to directly the attack of the enzyme-bound Hg^{2+}. The moderate acidity of the thiol, however, allows it to transfer a proton to one of the Hg^{2+} ligands (either Cys159 or Asp 99), in a process which both weakens the ligand-to-metal bond and transforms the thiol into a (much more nucleophilic) thiolate (Figure 2). Proton transfer to Cys159 (Figure 2B) occurs with a small barrier (12.3 – 12.8 $kcal.mol^{-1}$ in MP2, 7.8 – 8.0 $kcal.mol^{-1}$ using DFT) and is moderately exergonic by 7 – 9 $kcal.mol^{-1}$.

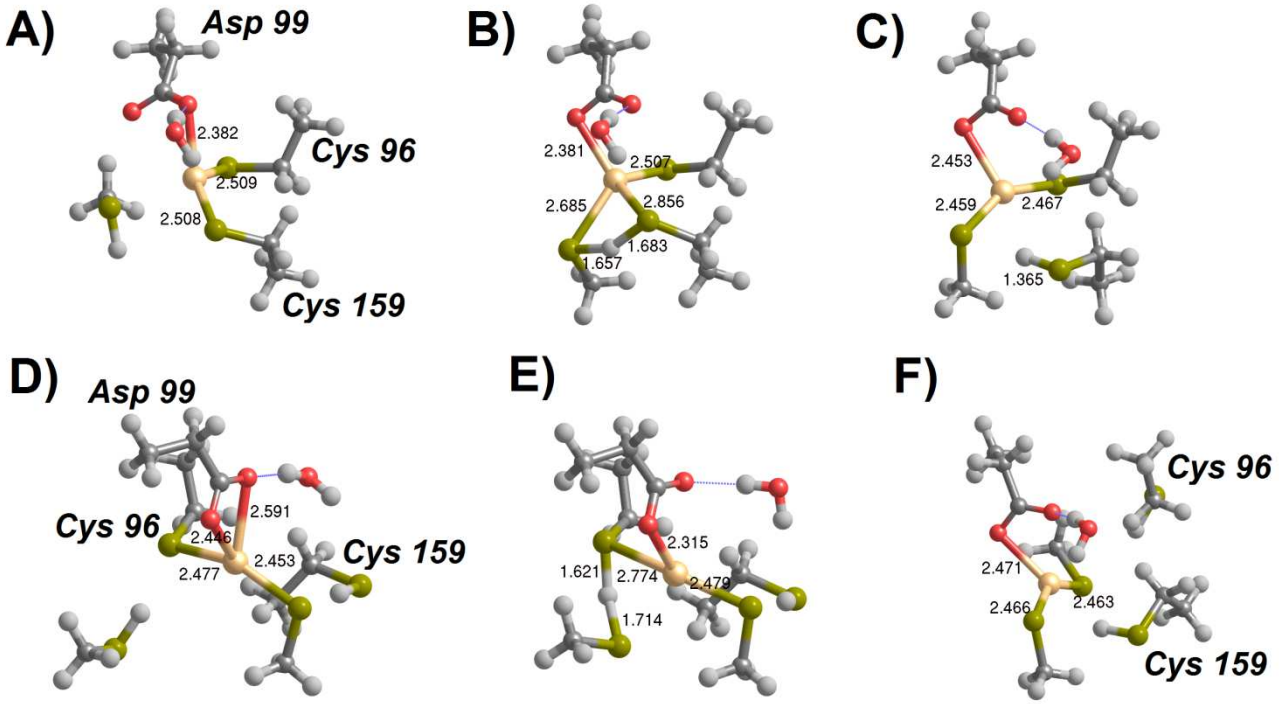

Figure 2: Cys-assisted thiol addition to Hg^{2+}. A) pre-reactional complex (Int1); B) H^+ transfer to Cys 159 (transition state); C) Thiol-based Int2 (Cys96-bound). D) Thiol-based Int2 (Cys96- bound) + CH_3SH; E) H^+ transfer to Cys 96 (transition state); F) Thiol-based Int4 (Asp99-bound). Relevant distances (in ångstrom) are highlighted.

Addition of a second thiol to the singly-cysteinated Hg^{2+} is quite similar to that of the first thiol, as expected from the identical composition of coordination sphere around the metal atom (a carboxylate and two thiols). The most interesting difference arises from the possibility of proton transfer to Cys96 (in the Cys96-bound Int2) due to the newly-found flexibility of the freed Cys159 sidechain. This step (Figure 2D-F) has a larger barrier (15.8 – 18.1 kcal.mol^{-1} using MP2, 14.5 – 14.8 kcal.mol^{-1} in DFT) than the addition of the first thiol because the larger thiol(ate)-Hg distance in the latter transition state (2.875 vs 2.685 Å) entails a smaller stabilization due to lower overlap between thiol(ate) and Hg

orbitals. In the gas phase, regeneration of the active site through the removal of $Hg(SCH_3)_2$ from Asp99 leads to a continuous increase in electronic energy of approximately 26 kcal.mol^{-1}. In solution, however, the reaction is only moderately endergonic (1 – 6 kcal.mol^{-1},depending on the dielectric constant) since the presence of a compact negative charge in the Asp99 residue in the product state leads to a stronger solvation of the separated fragments, which largely offsets the gas-phase energy increase due to the severing of the Hg-carboxylate bond.

If the initial conformation of the attacking thiol, in contrast to that depicted in Figure 2, has the S-H bond aligned towards Asp99, H^+-transfer to Asp99 occurs instead, without any thermodynamic barrier (Figure 3A). This transfer is favorable by 15 kcal.mol^{-1} and may be followed by a further movement of the proton from Asp99 to the distal Cys96 Hg-ligand (Figure 3B), which is thus released from the metal (Figure 3C). This proton-transfer step has a moderate barrier around 12-14 kcal.mol^{-1}, and should therefore occur at arate similar to that of the direct protonation and removal of the Cys159 ligand depicted in the alternative mechanism above (Figure2A-C). Addition of a second thiol may again proceed in an Asp99-assisted fashion (Figure 3D-F): proton transfer from the thiol to the Asp99 ligand of the Cys159-bound Int2 is favored by 10 – 11 kcal-mol^{-1} but must now overcome a small barrier (4 kcal.mol^{-1}), in contrast to the barrier-free process observed when this movement is the first step of the reaction sequence.

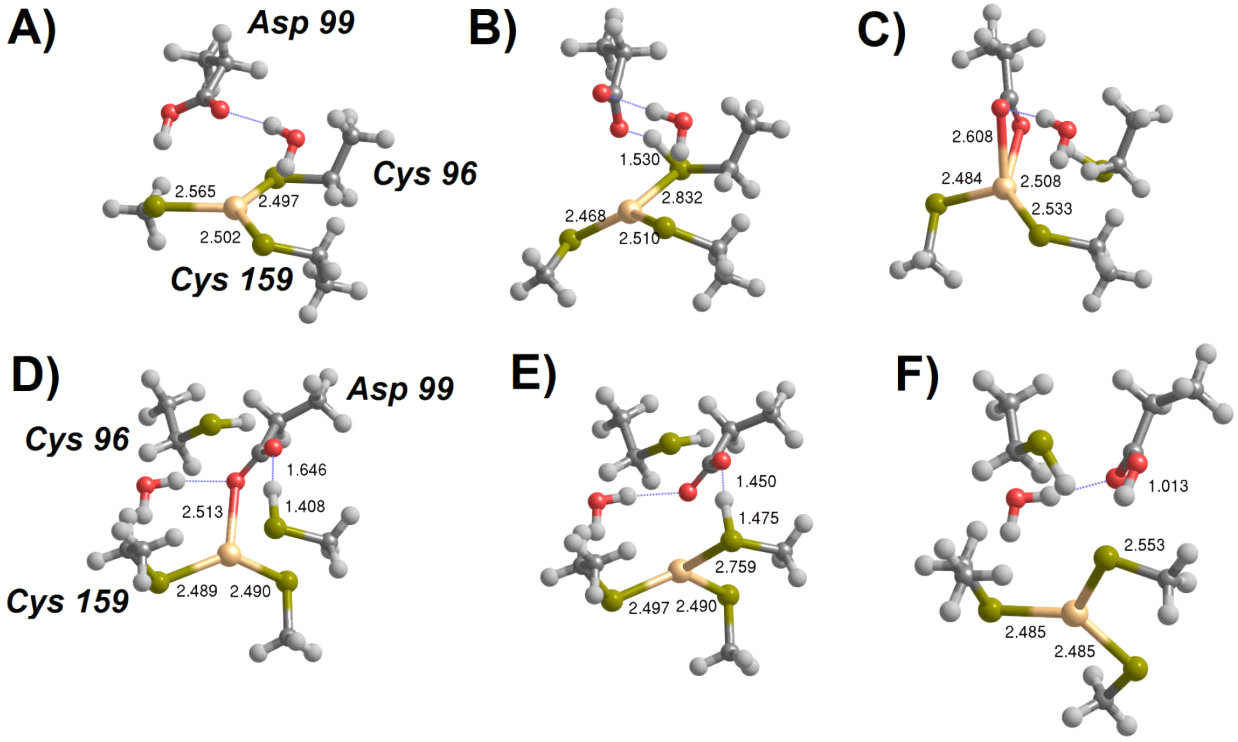

Figure 3: Asp99-assisted thiol addition to Hg^{2+}. A) Asp 99 receives H^+ from the attacking thiol. B) H^+ transfer from Asp99 to Cys96 (transition state). C) Thiol-based Int2 (Cys159-bound). D) Thiol-based Int2 (Cys159-bound) + CH_3SH. E) H^+ transfer from thiol to Asp99 (transition state). F) Thiol-based Int4 (Cys159-bound). Molecules D-F are depicted as seen from a point of view approximately opposite that used in the depiction of molecules A-C. Relevant distances (in ångstrom) are highlighted.

117

118 Table 1: Relative enthalpies (kcal.mol^{-1}) of the reaction intermediates in the Cys-assisted thiol addition to MerB-bound Hg^{2+}, computed at

119 the MP2/CBS // B3PW91/6-31G(d) level of theory.

	ε=4	ε=10	ε=20	ε=78.36
Reagent + CH_3SH	0.0	0.0	0.0	0.0
Int 1	-0.6	-1.2	-1.5	-1.7
TS Int1 to Int2 (Cys-96 bound)	11.7	11.4	11.3	11.1
Int2 (Cys-96 bound)	-8.3	-9.3	-10.0	-10.8
Int2 (Cys-96 bound)+ CH_3SH	-11.8	-12.4	-13.1	-14.0
TS Int2 to Int4	4.1	4.4	4.4	4.2
Thiol-based Int4 (Asp99-bound)	-12.8	-12.8	-13.5	-14.3
Infinitely separated products	-7.3	-10.7	-12.1	-13.3

120

121

Table 2: Relative enthalpies (kcal.mol^{-1}) of the reaction intermediates in the Asp99-assisted thiol addition to MerB-bound Hg^{2+}, computed at the MP2/CBS // B3PW91/6-31G(d) level of theory.

	ε=4	ε=10	ε=20	ε=78.36
Reagent + CH_3SH	0.0	0.0	0.0	0.0
Int 1 (protonated Asp99)	-15.4	-15.2	-15.2	-15.2
TS Int1 → Int2 (H^+ moves from Asp99 to Cys96)	-1.7	-2.4	-2.8	-3.2
Int 2 (Cys-159 bound)	-1.0	-0.9	-1.0	-1.1
Int 2 (Cys-159 bound) + CH_3SH	-9.6	-8.6	-8.3	-8.2
TS Int2 (Cys-159 bound) to Int4 (Cys159-bound).	-5.5	-4.7	-4.5	-4.4
Thiol-based Int4 (Cys159-bound)	-19.8	-19.4	-19.4	-19.5

128

In contrast to the addition of thiols analyzed above, addition of a thiolate to the MerB-bound Hg^{2+} proceeds unhindered, i.e. without any energetic barrier. The tetra-coordinated intermediate formed (Int1) lies 12 – 13 kcal.mol^{-1} below the infinitely-separated reactants (in MP2; 6 – 7 kcal.mol^{-1} below reactants in DFT), and may then shed any of its Cys-ligands upon overcoming a moderate 14.0 – 15.5 kcal.mol^{-1} barrier. Addition of a second thiolate to this complex, however, is much costlier due to the electrostatic repulsion between the freed, deprotonated, Cys and the negatively-charged thiolate. The precise cost depends very steeply on the chosen dielectric constant (Table 3), as expected for a reaction involving highly localized charges, but the transition state for this step always remains more than 25 kcal.mol^{-1} above Int1, far above the 16 –20 kcal.mol^{-1} expected(Parks et al., 2009) for the rate-limiting step of this enzyme from the application of the Eyring equation, $k_{cat} = \frac{k_B T}{h} e^{-\frac{\Delta G^{\ddagger}}{RT}}$, to the experimentally observed reaction rate(Begley et al., 1986b).

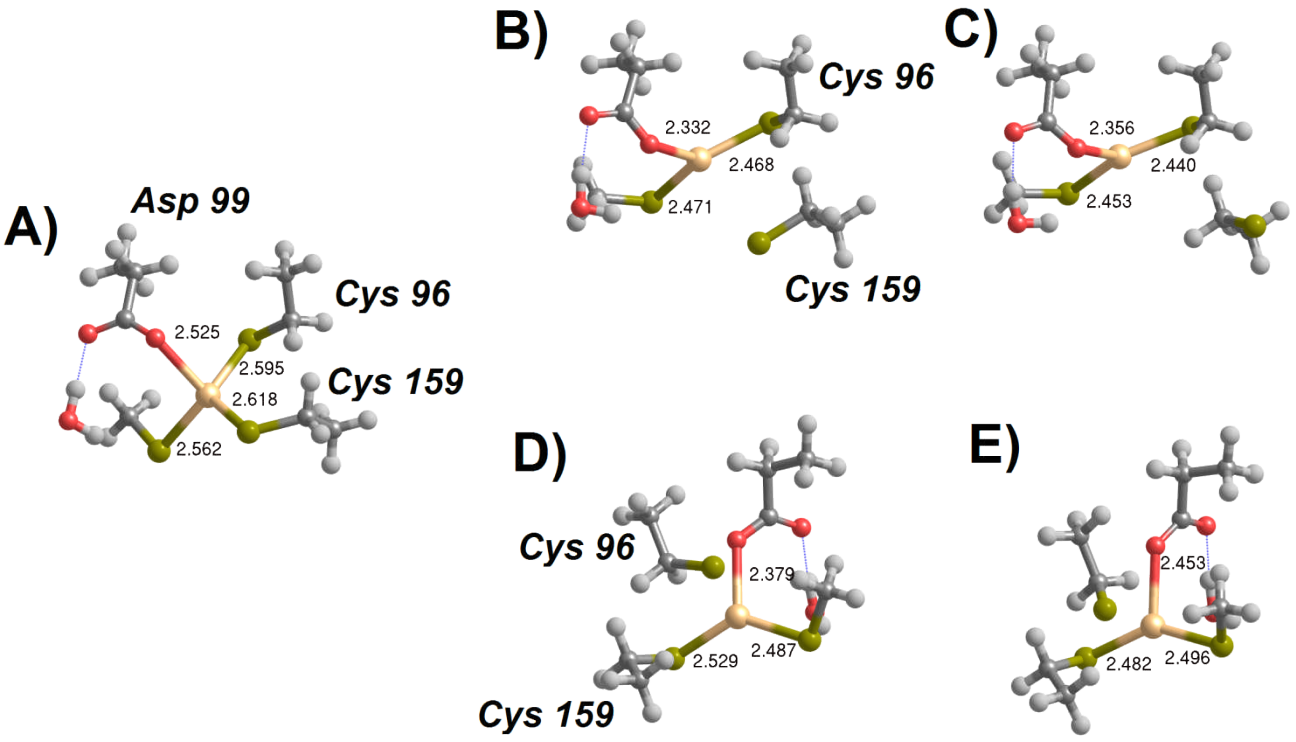

Figure 4: Addition of deprotonated thiol to MerB-bound Hg^{2+}. A) Thiolate-based Int1. B) breaking the Cys159-Hg bond (transition state). C) Thiolate-based Int2 (C96-bound). D) breaking the Cys96-Hg bond (transition state) E) Thiolate-based Int2 (C159-bound) Molecules E-F are depicted as seen from a point of view approximately opposite that used in the depiction of molecules A-C. Relevant distances (in ångstrom) are highlighted.

149 Table 3: Relative enthalpies (kcal.mol^{-1}) of the reaction intermediates in thiolate addition to MerB-bound Hg^{2+}, computed at the

150 MP2/CBS // B3PW91/6-31G(d) level of theory.

	ε=4	ε=10	ε=20	ε=78.36
Reactant + CH_3S^-	0.0	0.0	0.0	0.0
Thiolate-based Int1	-13.1	-12.6	-12.3	-12.1
Thiolate-based TS 1 →2 (C96-bound)	1.8	1.8	1.8	1.9
Thiolate-based Int2 (C96-bound)	-3.7	-2.6	-2.2	-1.9
Thiolate-based Int2 (C96-bound) + CH_3S^- TS	26.8	17.1	14.0	11.8
Thiolate-based Int3 (C96-bound)	10.6	1.5	-1.3	-3.2
Reactant + CH_3S^-	0.0	0.0	0.0	0.0
Thiolate-based Int1	-13.1	-12.6	-12.3	-12.1
Thiolate-based TS 1 →2 (C159-bound)	1.5	2.4	2.8	3.2
Thiolate-based Int2 (C159-bound)	-0.6	0.5	1.0	1.5
Thiolate-based Int2 (C159-bound) + CH_3S^- TS	32.3	21.0	17.3	14.6
Thiolate-based Int3 (C159-bound)	14.3	3.4	-0.1	-2.5

151

So far, we have only described the reaction mechanism arising from the addition of two thiols with the same protonation state. We now turn to the analysis of mechanism involving distinct protonation states of the attacking thiols: inded, the two N-terminal cysteines of MerA which catalyze removal of Hg^{2+} from MerB *in vivo* (Ledwidge et al., 2005) have been shown to possess widely separated pK_a's (Ledwidge et al., 2010) which entail that at physiological pH one of them is expected to remain mostly unprotonated while the other only deprotonates at high pH.

Addition of a thiolate to any of the forms of thiol-based intermediate 2 (where Hg^{2+} is bound to either of Cys159 or Cys96) occurs spontaneously without any energetic barrier. In the Cys159-bound form the reaction product has a slightly lower energy than in the Cys96-bound form and adopts a more exposed conformation (Figure 5, panel D). The metal ion in the resulting intermediate 3' has a sulfur-only coordination sphere in both instances, as the interactions with Asp99 have disappeared (Figure 5). Like the thiol-based intermediate 2, the *thiolate*-based intermediate 2 is susceptible to attack by a thiol in an Asp99-dependent manner. As in the other Asp99-assisted thiol attacks analyzed above, the electronic barrier to this process is negligible (Figure 5, panel C) and yields an intermediate where Asp99 is protonated and the mercury ion remains coordinated by three ligands (two external thiolates and Cys159). This Cys159-bound/Cys96-deprotonated/Asp99-protonated intermediate ($Int3_a$' in Figure 5, panel E) spontaneously decays, through a negligible energetic barrier (< 1 $kcal.mol^{-1}$), to the Cys159 bound/ Cys96-protonated/Asp99-deprotonated state. The overall reaction barrier for all of the mechanisms involving attack of the Hg^{2+} ion by a thiol and a thiolate therefore depends on the barrier of the first attack, which was computed above (Tables 1-3) to lie between 12 and 15 $kcal.mol^{-1}$ in all instances. Since the 3-4 $kcal.mol^{-1}$ difference between these barriers is equivalent to the intrinsic error of the computational protocols used, further discrimination between these three possibilities is unfortunately not possible at this stage.

175

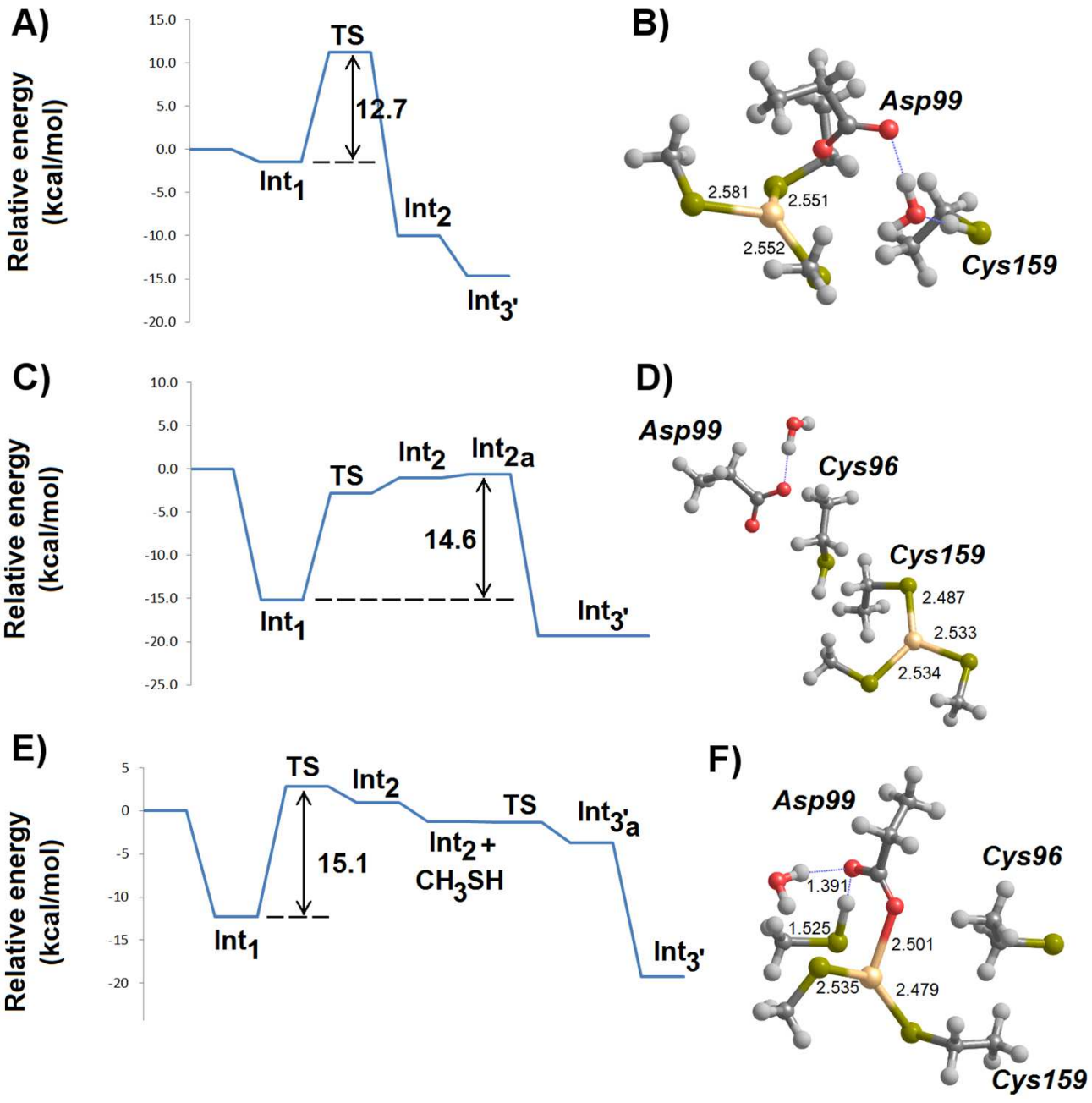

176

177 Figure 5: MP2/CBS//B3PW91/6-31G(d) energetic profiles (with ε=20) and representative structures
178 of intermediates arising from attack of Hg^{2+} by a thiol and a thiolate. A) Energetic profile of Cys159-
179 assisted thiol attack followed by thiolate addition; B) Structure of Int3' arising from Cys159-assisted
180 thiol attack; C) Energetic profile of Asp99-assisted thiol attack followed by thiolate addition; D)

Structure of Int3' arising from Asp99-assisted thiol attack followed by thiolate addition; E) Energetic profile of an initial thiolate attack followed by Asp99-assisted thiol addition to Hg^{2+}; F) Structure of the transition state of Asp99-assisted thiol addition to thiolate-based Int 2. Relevant distances (in ångstrom) are highlighted.

Regeneration of the initial state of the active site from the Int3' intermediate now requires the severing of the remaining Hg-Cys bond. Preliminary attempts at the characterization of this reaction step showed that direct stretching of the Hg-Cys bond is energetically quite costly. Our results above (Table 2), however, show that protonation of the metal-bound Cys dramatically weakens the Hg-S bond. We have therefore analyzed the feasibility of removing $Hg(SCH_3)_2$ from the active site cysteine through direct protonation by solvent-provided H_3O^+. A few explicit water molecules were also added to the model to provide an appropriate description of the solvated hydronium ion (Figure 6).

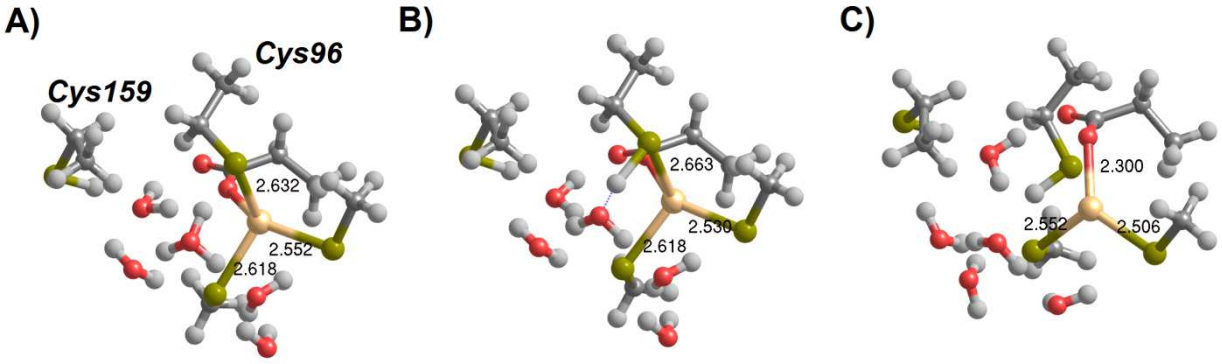

Figure 6: H_3O^+-assisted removal of $Hg(SCH_3)_2$ from the MerB active site (compact conformation). A) Cys96-bound Int3' surrounded by water-solvated H_3O^+; B) Proton transfer from H_3O^+ to Cys96 (Transition state); C) Asp-bound $Hg(SCH_3)_2$ (Int4). Relevant distances (in ångstrom) are highlighted

As mentioned above, two different conformations of the Int3' intermediate exist: an extended conformation (Figure 5D) where $Hg(SCH_3)_2$ is bound to Cys159 and a compact conformation where the product is bound to Cys96, instead (Figure 5B). In the compact conformation (Figure 6) this proton transfer is spontaneous by 6.6 $kcal.mol^{-1}$ (according to MP2; 2.7 $kcal.mol^{-1}$ according to DFT) and diffusion-controlled: the very small energetic barrier found during the geometry optimization completely disappears upon inclusion of solvation, zero-point and vibrational effects. Upon removal of Cys96, Asp99 weakly attaches to the mercury ion, preventing the product from freely diffusing away from the active site. Complete removal of $Hg(SCH_3)_2$ occurs upon stretching this very weak Asp-Hg bond.

In the "extended" conformation of Int3', the $Hg(SCH_3)_2$ moiety lies quite far from Asp99, which modifies the mechanistic analysis due to the impossibility of Asp99-attachment to the metal upon the release of Cys159. In contrast to the previous analysis, in this conformation the solvated H_3O^+ is unstable even before including bulk solvation effects implicitly through the PCM model. Instead, two separate minima arise: an unproductive intermediate featuring a proton on the Asp99 residue (Figure 7A), and the Cys159-protonated product featuring a free $Hg(SCH_3)_2$ (Figure 7C). Both minima lie 10 $kcal.mol^{-1}$ below the postulated initial (meta-stable) conformation featuring a solvated H_3O^+ (Figure 7B).

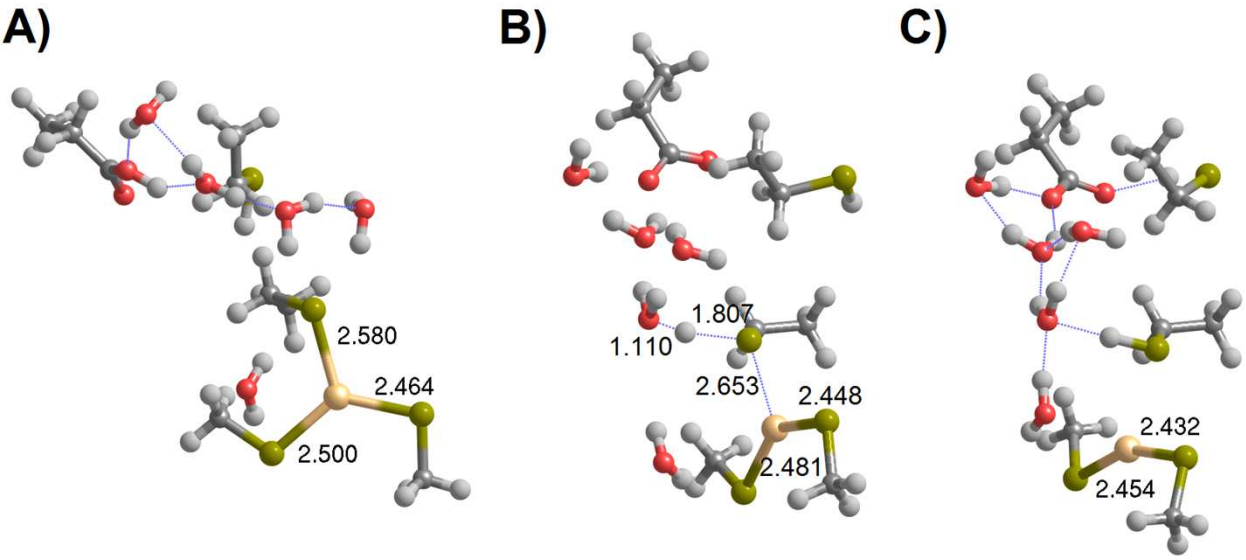

Figure 7: H_3O^+-assisted removal of $Hg(SCH_3)_2$ from the MerB active site (extended conformation). A) Asp99-protonated Int3' surrounded by water molecules; B) Proton transfer from Asp99 to Cys159 (Transition state); C) Regenerated active site with released $Hg(SCH_3)_2$. Relevant distances (in ångstrom) are highlighted

Discussion

Our computations show that the final steps of the reaction catalyzed by MerB, while conceptually simple, occur in a complex potential energy surface where several distinct pathways are accessible and may operate concurrently. The only pathway which clearly emerges as forbidden in our analysis is the one arising from the sequential addition of two thiolates to the metal atom, due to the accumulation of negative charges in the active site. Addition of two thiols, in contrast, leads to two feasible mechanistic possibilities. The most straightforward pathway proceeds through proton transfer from the attacking

thiol to Cys159 (activation ΔH=13 kcal.mol^{-1}), leading to its removal from the mercury coordination sphere, followed by a slower attack of a second thiol, which removes Cys96 (activation ΔH=16–18 kcal.mol^{-1}). Entropic effects, which we could not analyze due to the need of enforcing geometric constraints on our active site model, may, however, easily place this pathway above the experimentally determined activation ΔG (16 –20 kcal.mol^{-1}). The other pathway involves Asp99 in an accessory role similar to the one observed earlier for the initial stages of the reaction(Parks et al., 2009) and affords a lower activation enthalpy, around 14 kcal.mol^{-1}, determined solely by the cysteine removal step rather than by the thiol ligation step. Addition of one thiolate to the intermediates arising from either thiol attack occurs without a barrier and produces an intermediate (Int3') bound to one active site cysteine and from which $Hg(SCH_3)_2$ may be removed only after protonation by solvent-provided H_3O^+. This protonation event is quite spontaneous and occurs without an energetic barrier, making it subject only to H_3O^+ availability. Its activation energy in solution is therefore determined by the solution pH, and corresponds to $\Delta G^{\ddagger} = -RT \ln 10^{-pH}$.

Thiolate addition to the active site (prior to any attack by thiols) leads to pathways where the removal of the first cysteine becomes the rate-determining step (activation ΔH=14–15 kcal.mol^{-1}, irrespective of whether Cys159 or Cys96 leaves first). Asp99-assisted addition of a thiol to this intermediate then occurs without an energy barrier and yields the familiar Int3' intermediate discussed above.

A comparison of these results with the recently published computational analysis of the transfer of Hg^{2+} from the C-terminal cysteine pair of MerA to the buried cysteine pair in the active site of MerA(Lian et al., 2014) is very instructive. In that work, which included (unlike ours) the influence of the remainder of the enzyme through a QM/MM formalism, thiol addition to a Hg^{2+} ion coordinated by

two cysteines was observed to proceed through a relatively high-energy transition state (20.4 kcal.mol^{-1}) and to be endergonic by 9.0 kcal.mol^{-1}, in contrast to the 12-13 kcal.mol^{-1} barrier and 9-10 kcal.mol^{-1} exergonicity we computed for the related addition of a thiol to the MerB active site. Whereas the change in activation energy may be attributed to our neglect of the surrounding protein environment and to the absence, in the MerA study, of a direct proton transfer from the attacking thiol to the leaving Cys residue, further analysis points to another reason. Indeed, the QM-only results reported by Lian *et al.* in their Figure 7 show that neglect of the electrostatic influence of the protein brings the activation energy down to 12.6 kcal.mol^{-1} (in perfect agreement with our data) but only lowers the reaction energy by 10 kcal.mol^{-1} (instead of the 19 kcal.mol^{-1} needed for agreement with our study). This observation allows us to attribute this 9 kcal.mol^{-1} energy difference to the additional interaction, in MerB, of Asp99 with the mercury ion. The influence of Asp99 is also noticeable in the steps involving thiolate addition to mercury, which occur without a barrier in MerB but have an activation energy of 9 kcal.mol^{-1} in the QM-only MerA model and (in a smaller extent) in the removal of a cysteine from a thiolate-attacked mercury, which has an activation energy of 11 kcal.mol^{-1} in the QM-only MerA model, compared to 15 kcal.mol^{-1} in MerB.

References

Amovilli C, Mennucci B. 1997. Self-consistent-field calculation of Pauli repulsion and dispersion contributions to the solvation free energy in the polarizable continuum model. *The Journal of Physical Chemistry B* 5647:1051–1057.

Baker J, Kessi A, Delley B. 1996. The generation and use of delocalized internal coordinates in geometry optimization. *Journal of Chemical Physics* 105:192–212.

Barkay T, Miller SM, Summers AO. 2003. Bacterial mercury resistance from atoms to ecosystems. *FEMS Microbiology Reviews* 27:355–384.

276 Barone V, Bencini A, Totti F, Uytterhoeven MG. 1997. Comparison between post-Hartree-Fock and
277 DFT methods for the study of strength and mechanism of cleavage of Hg(SINGLE BOND)C
278 bond. *International Journal of Quantum Chemistry* 61:361–367.

279 Becke AD. 1993. Density-functional thermochemistry. III. The role of exact exchange. *The Journal of*
280 *Chemical Physics* 98:5648–5652.

281 Begley TP, Walts AE, Walsh CT. 1986a. Bacterial organomercurial lyase: overproduction, isolation,
282 and characterization. *Biochemistry* 25:7186–7192.

283 Begley TP, Walts AE, Walsh CT. 1986b. Mechanistic studies of a protonolytic organomercurial
284 cleaving enzyme: bacterial organomercurial lyase. *Biochemistry* 25:7192–7200.

285 Choi SC, Chase T, Bartha R. 1994. Metabolic Pathways Leading to Mercury Methylation in
286 Desulfovibrio desulfuricans LS. *Applied and environmental microbiology* 60:4072–7.

287 Cossi M, Mennucci B, Pitarch J, Tomasi J. 1998. Correction of cavity-induced errors in polarization
288 charges of continuum solvation models. *Journal of Computational Chemistry* 19:833–846.

289 Eto K, Marumoto M, Takeya M. 2010. The pathology of methylmercury poisoning (Minamata
290 disease). *Neuropathology : official journal of the Japanese Society of Neuropathology*:471–479.

291 Fox B, Walsh C. 1982. Mercuric reductase. Purification and characterization of a transposon- encoded
292 flavoprotein containing an oxidation-reduction-active disulfide. *J. Biol. Chem.* 257:2498–2503.

293 Küchle W, Dolg M, Stoll H, Preuss H. 1991. Ab initio pseudopotentials for Hg through Rn. *Molecular*
294 *Physics* 74:1245–1263.

295 Lafrance-Vanasse J, Lefebvre M, Di Lello P, Sygusch J, Omichinski JG. 2009. Crystal structures of the
296 organomercurial lyase MerB in its free and mercury-bound forms: insights into the mechanism of
297 methylmercury degradation. *The Journal of biological chemistry* 284:938–44.

298 Ledwidge R, Hong B, Dötsch V, Miller SM. 2010. NmerA of Tn501 mercuric ion reductase: structural
299 modulation of the pKa values of the metal binding cysteine thiols. *Biochemistry* 49:8988–98.

300 Ledwidge R, Patel B, Dong A, Fiedler D, Falkowski M, Zelikova J, Summers AO, Pai EF, Miller SM,
301 Conditions G. 2005. NmerA, the metal binding domain of mercuric ion reductase, removes Hg2+
302 from proteins, delivers it to the catalytic core, and protects cells under glutathione-depleted
303 conditions. *Biochemistry* 44:11402–16.

304 Di Lello P, Benison GC, Valafar H, Pitts KE, Summers AO, Legault P, Omichinski JG. 2004. NMR
305 structural studies reveal a novel protein fold for MerB, the organomercurial lyase involved in the
306 bacterial mercury resistance system. *Biochemistry* 43:8322–8332.

307 Li X, Liao R-Z, Zhou W, Chen G. 2010. DFT studies of the degradation mechanism of methyl mercury
308 activated by a sulfur-rich ligand. *Physical chemistry chemical physics : PCCP* 12:3961–71.

Lian P, Guo H-B, Riccardi D, Dong A, Parks JM, Xu Q, Pai EF, Miller SM, Wei D-Q, Smith JC et al. 2014. X-ray Structure of a Hg(2+) Complex of Mercuric Reductase (MerA) and Quantum Mechanical/Molecular Mechanical Study of Hg(2+) Transfer between the C-Terminal and Buried Catalytic Site Cysteine Pairs. *Biochemistry* 53:7211–22.

Lin C-C, Yee N, Barkay T. 2012. Microbial Transformations in the Mercury Cycle. In: Liu G, Cai Y, O'Driscoll N eds. *Environmental Chemistry and Toxicology of Mercury*. Wiley, 155–192.

Mennucci B, Tomasi J. 1997. Continuum solvation models: A new approach to the problem of solute's charge distribution and cavity boundaries. *Journal of Chemical Physics* 106:5151–5158.

Ni B, Kramer JR, Bell RA, Werstiuk NH. 2006. Protonolysis of the Hg-C bond of chloromethylmercury and dimethylmercury. A DFT and QTAIM study. *The journal of physical chemistry. A* 110:9451–9458.

Parks JM, Guo H, Momany C, Liang L, Miller SM, Summers AO, Smith JC. 2009. Mechanism of Hg-C protonolysis in the organomercurial lyase MerB. *Journal of the American Chemical Society* 131:13278–85.

Parks JM, Johs A, Podar M, Bridou R, Hurt RA, Smith SD, Tomanicek SJ, Qian Y, Brown SD, Brandt CC et al. 2013. The genetic basis for bacterial mercury methylation. *Science (New York, N.Y.)* 339:1332–5.

Perdew JP. 1991. Unified theory of exchange and correlation beyond the local density approximation. In: Ziesche P, Eschrig H eds. *Electronic Structure of Solids '91*. Physical Research. Berlin: Akademie Verlag, 11–20.

Peterson K a., Puzzarini C. 2005. Systematically convergent basis sets for transition metals. II. Pseudopotential-based correlation consistent basis sets for the group 11 (Cu, Ag, Au) and 12 (Zn, Cd, Hg) elements. *Theoretical Chemistry Accounts* 114:283–296.

Pitts KE, Summers AO. 2002. The Roles of Thiols in the Bacterial Organomercurial Lyase (MerB). *Biochemistry* 41:10287–10296.

Riccardi D, Guo H-B, Parks JM, Gu B, Summers AO, Miller SM, Liang L, Smith JC. 2013. Why Mercury Prefers Soft Ligands. *The Journal of Physical Chemistry Letters* 4:2317–2322.

Tomasi J, Persico M. 1994. Molecular Interactions in Solution: An Overview of Methods Based on Continuous Distributions of the Solvent. *Chemical Reviews* 94:2027–2094.

Truhlar DG. 1998. Basis-set extrapolation. *Chemical Physics Letters* 294:45–48.

Varekamp JC, Buseck PR. 1986. Global mercury flux from volcanic and geothermal sources. *Applied Geochemistry* 1:65–73.